Asian Journal of Chemistry; Vol. 33, No. 3 (2021), 583-590

ASIAN JOURNAL OF CHEMISTRY

https://doi.org/10.14233/ajchem.2021.23053

Nd-Doped Fe_3O_4 Nanoparticles: Microwave Synthesis, Catalytic Properties in Selective Oxidation of Styrene

V.T. GEETHA[1,2,*] and S. INDUJA[2]

[1]Department of Chemistry, Sri Sairam Engineering College, Sai Leo Nagar, West Tambaram, Chennai-600044 India
[2]Hindustan Institute of Technology and Science, No. 1, Rajiv Gandhi Salai (OMR), Padur, Chennai-603103, India

*Corresponding author: E-mail: geethavt@yahoo.com

Received: 5 November 2020; *Accepted*: 6 January 2021; *Published online*: 16 February 2021; AJC-20253

Nanocrystalline powder of neodymium substituted iron oxides samples were synthesized through the microwave approach. The synthesized pristine Fe_3O_4 and Nd-doped Fe_3O_4 structural properties were analyzed by the X-ray diffraction technique. The microstructural details, morphology and elemental composition were assessed by transmission and scanning electron microscopy attached with EDX. The Fe_3O_4 nanostructures possess spherical morphology as well as consistent particle size distribution, which is confirmed by HR-SEM. The formation of Fe_3O_4 with high purity was confirmed by EDX and XRD analysis. The particle size calculated by HR-TEM images and crystallite size through the XRD study showed that the value obtained by both the methods is nearly the same. The catalytic properties of Fe_3O_4 nanoparticles are examined in the selective oxidation of styrene.

Keywords: Neodymium, Iron oxides, Nanomaterials, Optical, Structural, VSM.

INTRODUCTION

Transition metal-doped oxides of magnetite (Fe_3O_4) have been used in various industrial applications, such as electro-chemical activity, magneto-resistance effect, hyperthermia and catalysis [1,2]. However in most of the applications, high magnetization is needed, it deteriorates considerably whenever dimensions are decreased from bulk size to nano range, as a result of surface impacts, in which magnetic order is extremely disturbed. Consequently, an improvement of magnetization in iron oxide nanostructures is indeed a difficulty to the researchers. The face-centered cubic structure formed by oxygen and the octahedral and tetrahedral sites is occupied by Fe cations as a result the cubic inverse spinel structure formed on Fe_3O_4 [3]. In the octahedral sites, the exchange of electrons can happen amongst the Fe^{3+} and Fe^{2+} ions at room temperature and thus the Fe_3O_4 behave as a metal partially.

It was described that the specific surface area, crystallography and morphology are the important parameters which decides the Fe_3O_4 catalytic performance. To maximize the catalytic performance many better synthesis techniques were formulated which includes metal doping, synthesizing with other materials, controllable morphology and particle size [4,5]. Though, the impact of neodymium doping on the lattice of Fe_3O_4 for improving magnetic properties and as a catalyst was not examined until now. In recent times, the microwave approach got significance compared to other appro-aches. In the microwave technique, the reactant molecules interacted by the microwaves at the molecular level and as a result, consistent heating obtained. Due to the motion of the molecules at the time of microwave combustion, the microwave energy is transformed into heat energy. As a result, the form-ation of Fe_3O_4 and Nd-doped Fe_3O_4 nanoparticles takes place within a short period of time [6].

The oxidation of styrene produces benzaldehyde, which is an important chemical compound in industries. One more major product generally formed alongside benzaldehyde is styrene oxide [7-9]. Hence, the oxidation to benzaldehyde with high selectivity continues to be difficult in the present industrial procedures as well as environmental risks and low yields also need to be addressed [10]. Compared to homogeneous catalytic oxidation, the most favourable approach is heterogeneous catalysis because of ease of removal from the reaction medium, retrieval and reusing for prolonged operation. For the above

reasons, the improvement of heterogeneous catalysts with eco-friendly reagents (for instance, oxidant and solvent) for liquid-phase selective oxidation has become more and more interesting. Many investigators have suggested that the concentration and substitution of rare-earth elements strongly influence the magnetic, catalytic and electrical properties of the spinel metal oxides [11-13]. These rare-earth distinct properties are likely to be arises from the electronic states of 4*f*-orbital. Therefore, it is meaningful to search the inherent relationship between catalysis and size/surface properties. The Nd-doped Fe_3O_4 oxides active sites were examined during the oxidation of styrene.

EXPERIMENTAL

Preparation: The following procedure is a typical process for synthesizing pristine and Nd-doped Fe_3O_4 nanoparticles. In the beginning, solutions of neodymium(III) nitrate hexahydrate and 0.01 to 0.05 molar ferric(III) nitrate hexahydrate (4.0 mL) were mixed together. In addition to that, a solution of urea (6.0 mL, 0.4 mol) was added to the above solution in a dropwised manner. Followed by, the above mixture was kept inside a household IFB 20SC2 microwave oven and then subjected to microwave irradiation for 10 min. The microwave oven having 2.450 MHz microwave frequency and 1200 Watts microwave energy. During the microwave combustion, the above homogeneous mixture begins to boil, accompanied by the evaporation occurs alongside the liberation of gases. If the chemical source mixture proceeds to an automated combustion state, the mixture will evaporate and, as soon as the solid forms. The final solid substance was effectively cleaned out by ethanol and then at 120 ºC dehydrated for 1 h. The samples and Nd-doped Fe_3O_4 (0.00 and 0.01 to 0.05) were designated as (a) and (b) to (e).

Characterization: The pristine alongside Nd-doped Fe_3O_4 samples X-ray diffraction patterns were analyzed with an instrument called X-ray diffractometer (Maker: Rigaku) by using CuKα radiation. Scanning electron microscopy with higher resolution (HR-SEM) pictures acquired through Philips XL30 ESEM microscope attached together with energy-dispersive X-ray spectroscopy. Transmission electron microscopy having higher resolution (HR-TEM) pictures were recorded using a transmission electron microscope (Philips EM 208) powered with 200 kV accelerating voltage. The Cary Eclipse Fluorescence spectrophotometer and Cary 100 UV-visible spectrophotometer was used for recording optical properties and diffuse reflectance spectra of pristine Fe_3O_4 and Nd-doped Fe_3O_4 samples. Room temperature magnetic measurements recorded using a vibrating sample magnetometer (Manufactured by and Model No.: Riken Danish Company Ltd., Japan and BHV-50).

RESULTS AND DISCUSSION

XRD analysis: The X-ray diffraction patterns of Nd-doped Fe_3O_4 (0.01 to 0.05%) nanoparticles are shown in Fig. 1a. The samples recorded between 25-75º 2θ range at room temperature. The pristine and Nd-doped Fe_3O_4 samples diffraction peaks, as well as relative intensities, well match with the JCPDS No. 33-0664. The tetrahedral sites (up to $x = 0.01$) were occupied by Nd ions. Though, the Nd^{3+} ions became available on both the octahedral and tetrahedral sites when an increase of Nd^{3+} substitutions further (Fig. 1b). However, significant changes in the direction of lower angles are noticed for most sharp peaks by doping. This sort of change shows a lattice expansion effect because of the substitution of Nd crystal lattice. The modifi-cation in peak intensities is especially due to the distinction in Nd and Fe content in spinel oxides. The indexing of peaks is made through the use of *d*-values. The highest top having hkl value indicates the crystal structure. Inside the oxides, Nd and Fe ions migrated to the octahedral and tetrahedral position accordingly results in the change in peak intensities [14,15]. Apart from peak shifting, the peak intensities found become decreased as well as the full-width-at-half-maximum (FWHM) becomes higher as a result of doping Nd atoms on Fe sites (Fig. 1b), which is described as due to reduction of grain size by incorporation of rare-earth atoms [16]. The 2θ shifts to a smaller angle and the corresponding lattice constant decreases from 8.412 $Å^3$ to 8.386 $Å^3$. This demonstrates that a small part Fe^{2+} (ion radius = 0.61 nm) and Fe^{3+} (ion radius = 0.49 nm) in the Fe_3O_4 are occupied by Nd with a larger ion radius of 0.0983 nm to form Nd-doped Fe_3O_4. No peaks of other impurities, metal hydroxides or hematite had been noticed. This confirmed the formation of pure Fe_3O_4. The sharp and intense peaks showed that Fe_3O_4 nanoparticles possess better crystallinity and maximum purity.

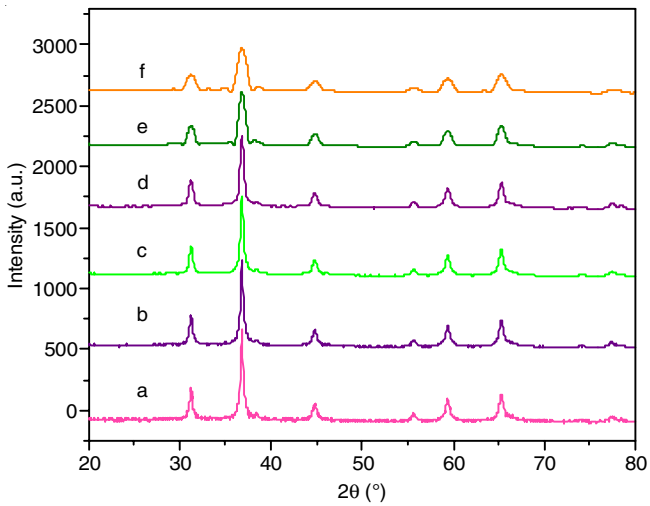

Fig. 1a. XRD pattern of undoped Fe_3O_4 and Nd-doped (0.01, 0.02, 0.03, 0.04 and 0.05%) Fe_3O_4

By using the Scherrer's formula and from the diffraction peaks, the mean crystallite size of pristine and Nd-doped Fe_3O_4 samples was calculated [17] using the following formula:

$$L = \frac{0.89\lambda}{\beta\cos\theta}$$

where, L = average crystallite size (Å), λ = wavelength of the incident X-ray beam (1.54 Å), β = the FWHM (rad) and θ = is the Bragg's angle. The average crystallite size was 22.11 and 15.98 nm for samples, respectively (Fig. 1c). In the same way, the dislocation line density and the microstrain have the same trend depicting the reduction of defect density.

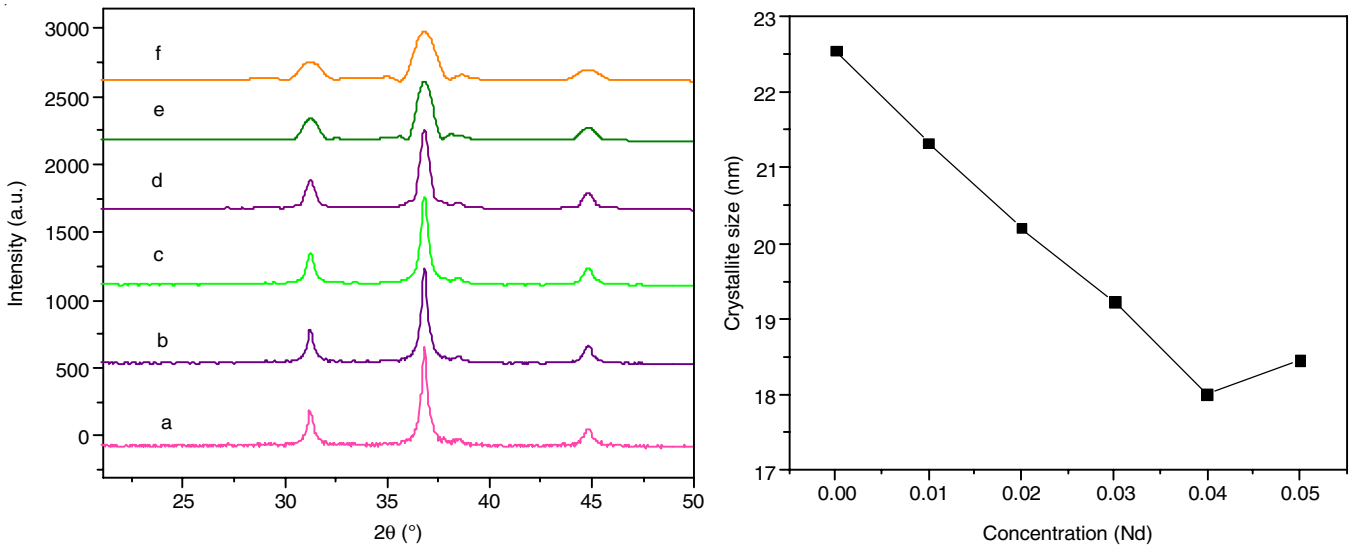

Fig. 1b. XRD pattern of (2θ value 20-50) undoped Fe_3O_4 and Nd doped Fe_3O_4

Morphology analysis: Fig. 2a-f show the HRSEM images of Nd-doped Fe_3O_4 (x = 0.01-0.05%) samples. The samples exhibited a compact arrangement of homogeneous spherical shaped nanoparticles with smaller agglomeration and with a diameter ranging below 15-24 nm. The HRSEM images of Nd-doped Fe_3O_4 samples also confirmed the presence of agglomerated microcrystals. The observed agglomeration of nanostructures is mainly due to the presence of magnetic interactions among the materials. Therefore, it can inferred that agglomerated Nd-doped Fe_3O_4 nano- and microcrystals have been formed during the heating process in the microwave method, respectively.

From the HRTEM images (Fig. 3a-f), it can be found that undoped Fe_3O_4 nanoparticles and Nd-doped Fe_3O_4 crystalline and the distance between the particle size 23.45 nm (Fe_3O_4-undoped) and Nd-doped Fe_3O_4 particle size decreases 14.22 nm (0.01 to 0.05%), respectively, which is in accordance with the (3 1 1) lattice fringes in the inverse spinel Fe_3O_4 nanoparticles [18], which is in agreement with the XRD results.

The presence of Nd-doped Fe_3O_4 (x = 0.01 to 0.05) was also confirmed by means of energy dispersive X-ray analysis (EDX) as shown in Fig. 4a-f. It exhibited Nd, Fe and O peaks and indicated the presence of Nd-doped Fe_3O_4 (x = 0.01 to 0.05) phase without any other impurity. The peaks at 2.1, 10.11 and 12.2 keV in the EDX spectra were due to the gold-coated on the samples before recording HRSEM analysis for better visibility of the surface morphology.

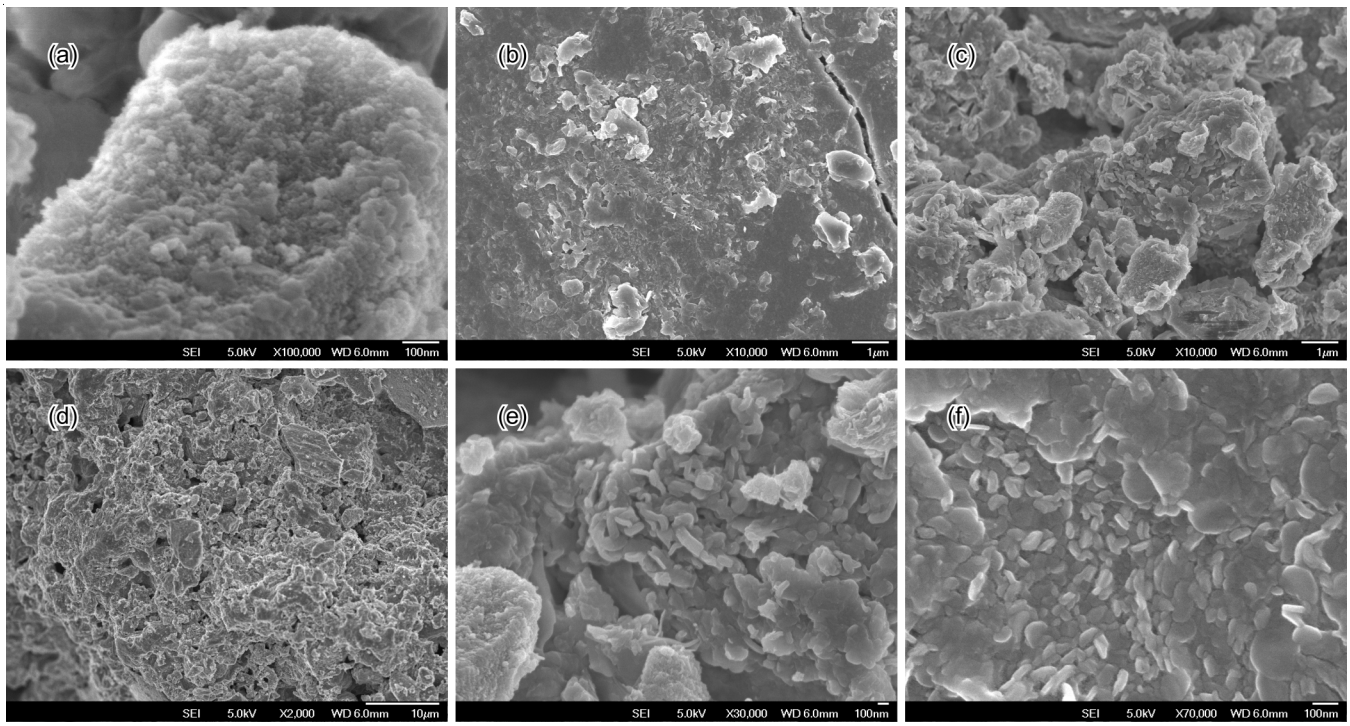

Fig. 2. HR-SEM images of undoped Fe_3O_4 and Nd-doped (0.01, 0.02, 0.03, 0.04 and 0.05%) Fe_3O_4

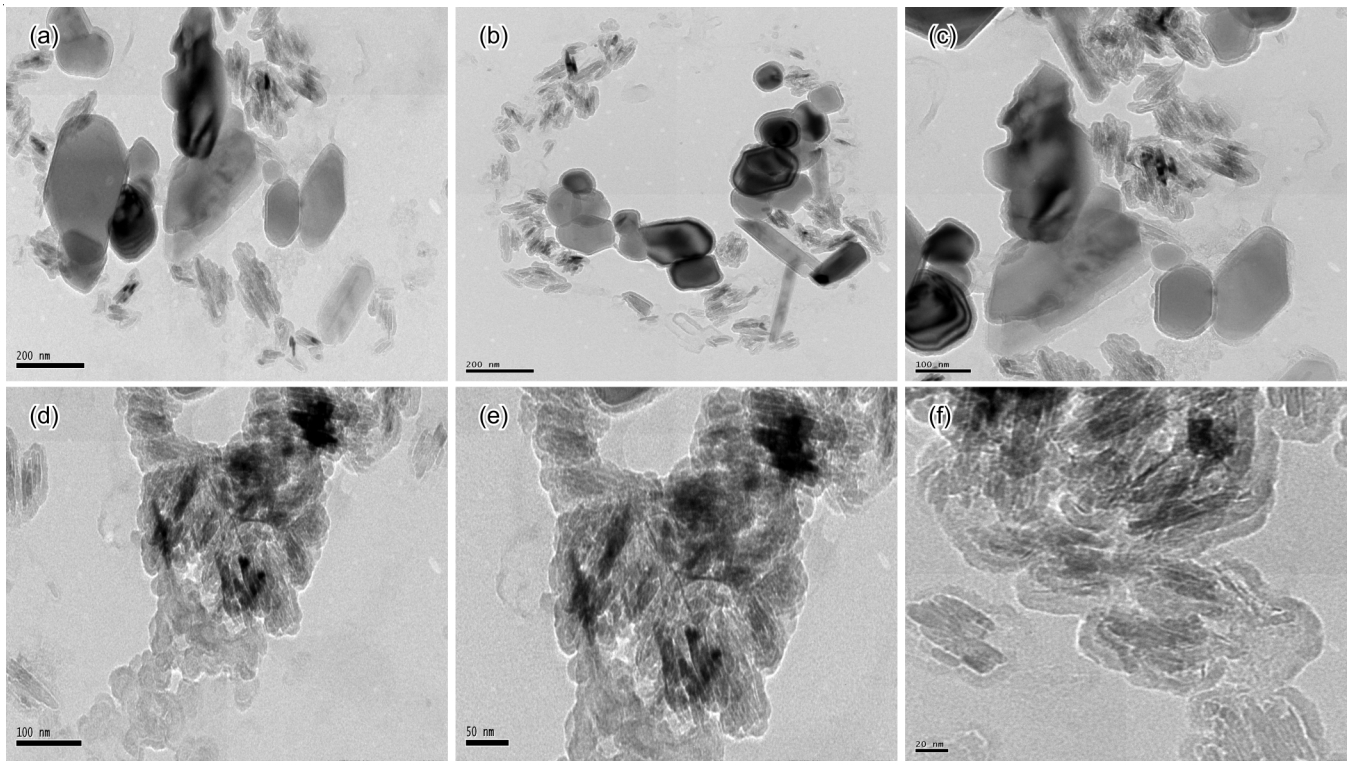

Fig. 3. HR-TEM images of undoped Fe_3O_4 and Nd-doped (0.01, 0.02, 0.03, 0.04 and 0.05%) Fe_3O_4

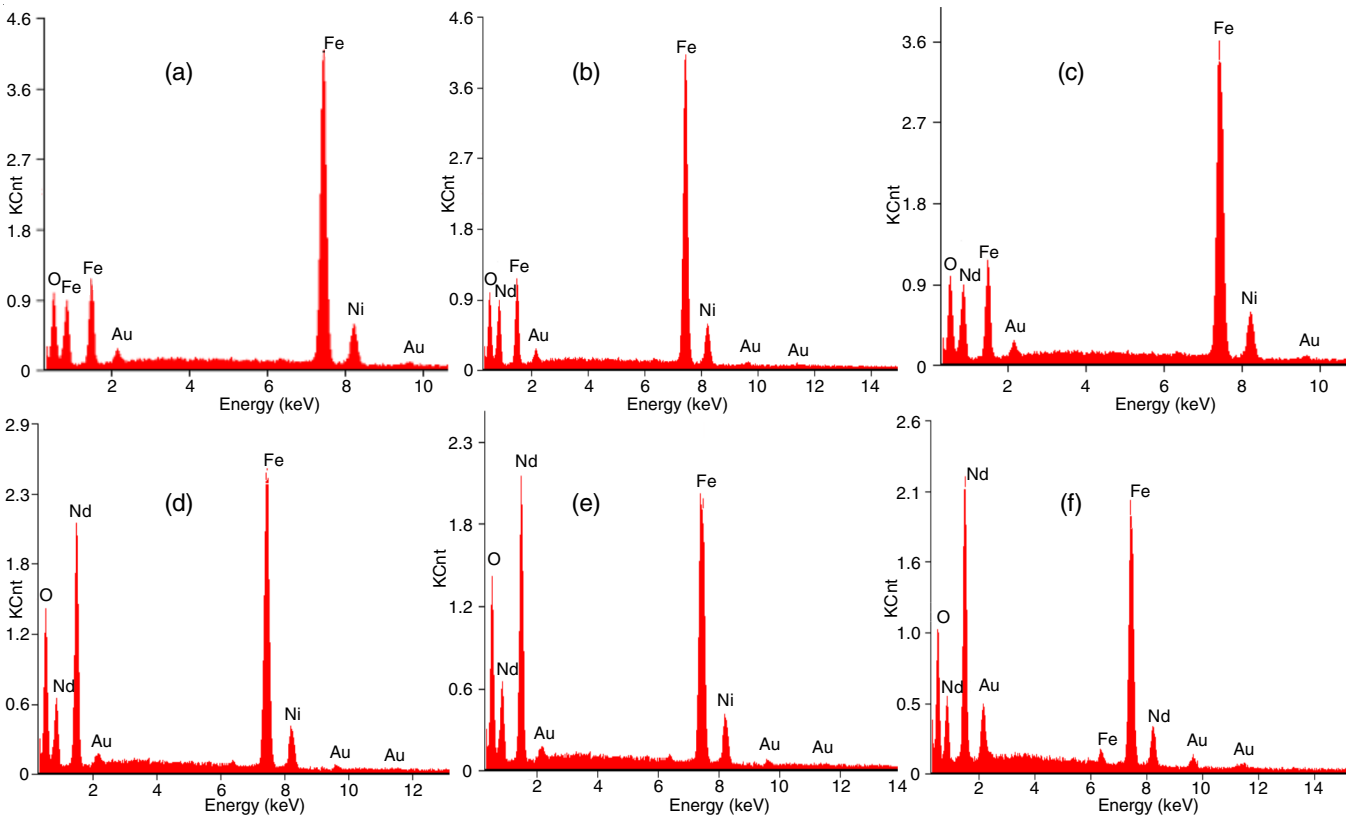

Fig. 4(a-f) EDX spectra of undoped Fe_3O_4 and Nd-doped (0.01, 0.02, 0.03, 0.04 and 0.05%) Fe_3O_4

Diffuse reflectance spectroscopy (DRS) studies: The pristine and Nd-doped Fe_3O_4 nanoparticles' optical properties were examined with the help of UV-visible diffuse reflectance spectroscopy (DRS). The pristine and Nd-doped Fe_3O_4 samples bandgap could be examined through the E_g measurements by making use of Kubelka-Munk (K-M) model [19,20] and also the F(R) was calculated by applying the following formula:

$$F(R) = \frac{(1-R)^2}{2R}$$

where F(R) is the Kubelka-Munk function and R is the reflectance.

The bandgap value was calculated from the intercept value by plotting a graph with the functions of hv and $[F(R)hv]_2$ and the graph is displayed in Fig. 5. The bandgap of pristine Fe_3O_4 is 1.18 eV and the bandgap found between 2.12 to 2.25 eV for Nd-doped Fe_3O_4, which confirms that there is an increase in the bandgap after doping. Sahana *et al.* [21] described the Fe_3O_4 nanoparticles bandgap as 2.62 eV, which can be blue-shifted in comparison to Nd-doped Fe_3O_4. As observed from the reflection spectra, a sharp absorption part shifted in the direction of the longer wavelength region when the amount of Nd increases, resulting in a reduction of the optical bandgap. In the same way, the doping levels can combine along with the valence or conduction band and besides, they became a state of band tail during the more substantial levels of doping, which leads to a reduction of crystal size [22,23]. A relationship between the nanocrystallite size and the bandgap values with regards to the confinement effect, because of the iron oxide nanocrystallites size. It is proved that the bandgap of Nd-doped Fe_3O_4 nanoparticles reduces from 2.12 to 2.05 eV with increasing the particle size of iron oxide samples (Fig. 5b).

Photoluminescence studies: Photoluminescence (PL) spectra give significant details, for instance, oxygen vacancies, surface states and defects, separation of charge carrier and a process of recombination in nanosize semiconductor materials induced by photons. Furthermore, a type of photoluminescence spectral range of pure Fe_3O_4 and Nd-doped Fe_3O_4 will depend upon the synthesis approaches (Fig. 6). A wide emission band is noticed and located between 420-530 nm for pure Fe_3O_4 and Nd-doped Fe_3O_4, which can be because of the defects of the intraband gap, such as oxygen vacancies. On the other hand, the emission bands intensity reduction and quite a bit blue shifted, because of the decrease in the mean crystallite size that can be in good agreement with all the results acquired by XRD information. The photoluminescence intensity is impacted by the defects present at the surface as well as the number of times the chargers getting transferred. Furthermore, the emission peaks most likely shifted to the longer wavelength location as a result of increased reaction time that can be because of the nanostructures formation impact along with the nanoparticle size increases (Fig. 6). Consequently, the electrons in the valence band are most probably excited in direction of the intermediate states; later, a comparatively intense blue-green luminescence producing [24,25]. In this present study, undoped Fe_3O_4 and Nd-doped Fe_3O_4 nanoparticles had been prepared by combustion techniques. In general, combustion techniques are fast crystallization, complete oxidation and quick evaporation may produce many structural defects, for instance, oxygen vacancy and will act as strong defect donors in the semiconductor oxide and would cause the forming of newer energy levels within the bandgap of pristine Fe_3O_4 and Nd-doped Fe_3O_4. The purpose of the current study would be to create thorough research on the dependence of magnetic and optical properties of pristine Fe_3O_4 and Nd-doped Fe_3O_4 nanoparticles on a relative with the preparation methods.

Vibrating sample magnetometer (VSM) hysteresis loop analysis: A VSM hysteresis loop defines the pristine Fe_3O_4 and Nd-doped Fe_3O_4 nanoparticles' magnetic properties. It is

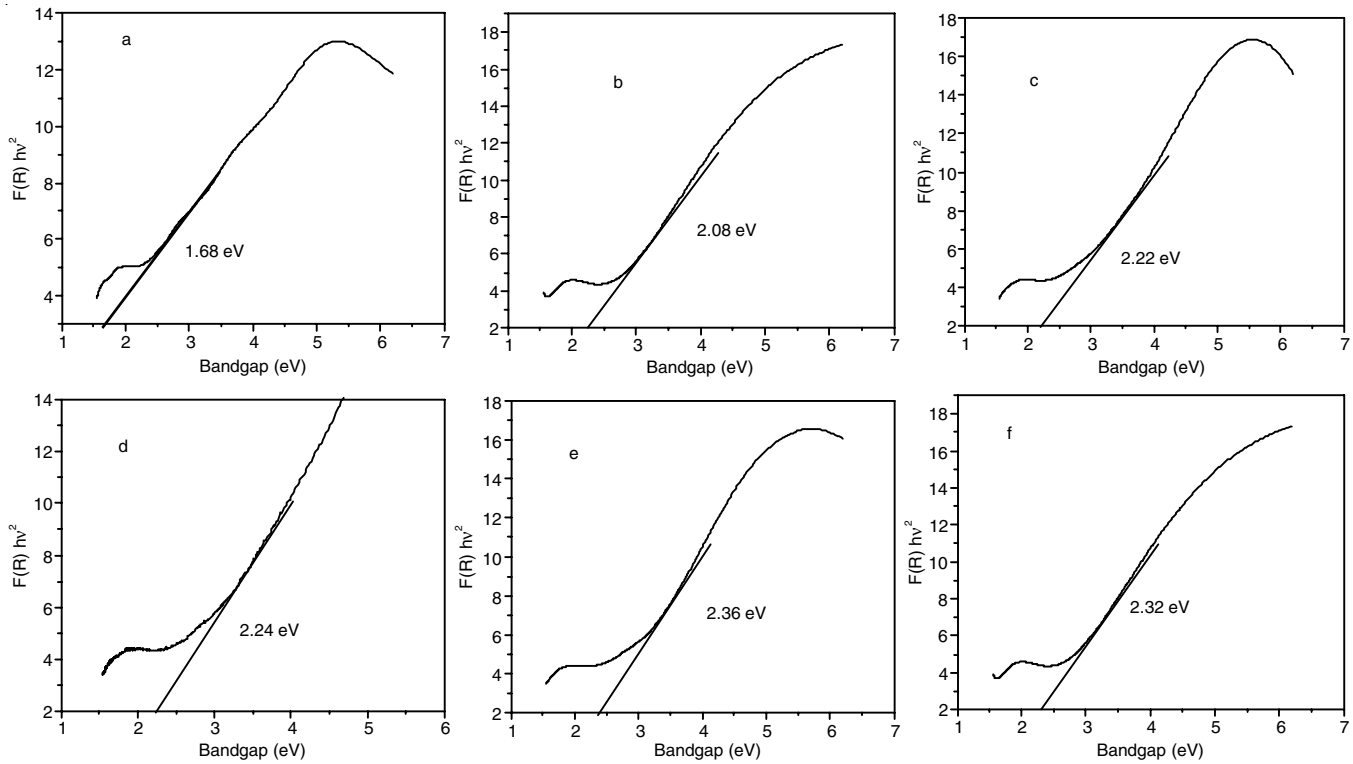

Fig. 5. DRS spectra of bandgap undoped Fe_3O_4 and Nd-doped (0.01, 0.02, 0.03, 0.04 and 0.05%) Fe_3O_4

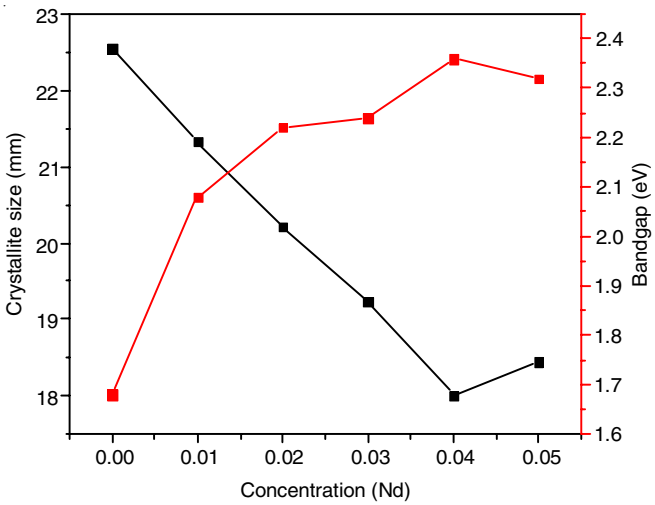

Fig. 5b. Particle size of iron oxide samples

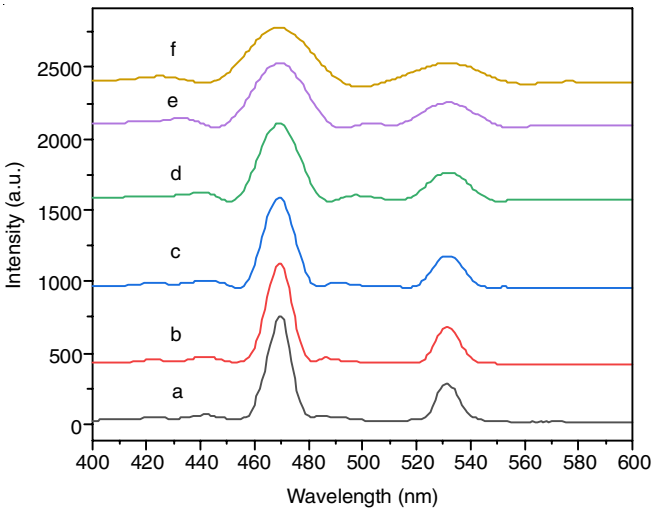

Fig. 6. Photoluminescence spectra of undoped Fe_3O_4 and Nd-doped (0.01 to 0.05%) Fe_3O_4

performed with the help of a vibrating sample magnetometer having the energy between -10 kOe to +10 kOe and also the results are presented in Fig. 7. All of the Nd-doped Fe_3O_4 (0.01 to 0.05%) nanoparticles showed a hysteresis loop and therefore are perhaps not well resolved and proved the superparamagnetic nature of the nanometal oxides. The room temperature magnetic hysteresis loops showed the superparamagnetic (SP)-ferromagnetism (FM) behaviour of all the samples except for pristine Fe_3O_4. The changes in magnetic parameters in accordance with the difference in the ratios of nano-oxides. The total magnetic response for the pure oxide and mixed metal oxide is based on the volume fraction of the metal oxides, because of the magnetic agent, as well as on the share of the magnetic pristine Fe_3O_4 and Nd-doped Fe_3O_4 to the total magnetization. Furthermore, superparamagnetic to ferromagnetic arises usually in ferromagnetic nanoparticles with a size between 15-20 nm. The pristine Fe_3O_4 and Nd-doped Fe_3O_4 had been superparamagnetic-ferromagnetic in nature. Whenever it merges with Nd-Fe and is reduced into the nano-region at room temperature, there can be a reduction in magnetization and displays superparamagnetism behaviours [25]. The Fe_3O_4 magnetic nature

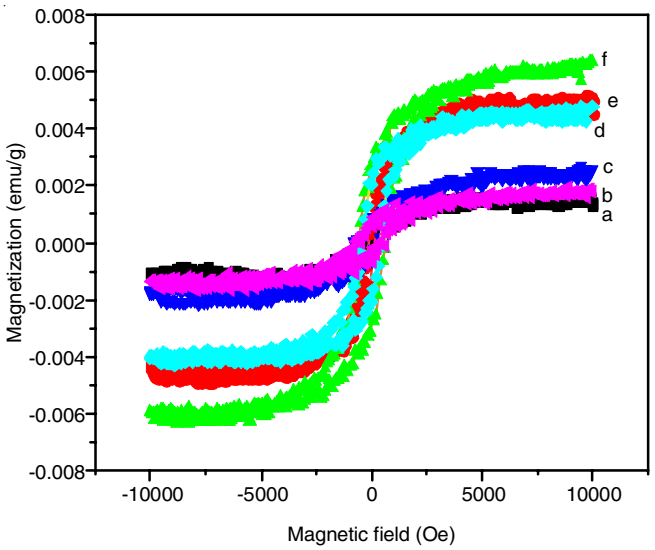

Fig. 7. VSM spectra of undoped Fe_3O_4 and Nd-doped (0.01, 0.02, 0.03, 0.04 and 0.05%) Fe_3O_4

is activated by Fe^{2+} cations because of Fe^{3+} cations are located in both octahedral as well as tetrahedral sites in the crystal lattice and besides orient in opposition to one another. The octahedral site pointed in the direction of an applied magnetic field, whereas the tetrahedral site pointed in the opposite direction of the applied magnetic field, thus Fe^{3+} magnetic moments become neutralized. Within the framework of inverse spinel, the tetrahedral sites are smaller compared to octahedral sites, because of this, Nd^{3+} ions prefer to go for octahedral B-site as well as the Nd^{3+} ions exchanged the Fe^{3+} ions.

As displayed in Table-1, the retentivity (M_r) and coercivity (H_c) values reduce when the chromium ion percentage raises, which leads to the ferromagnetism behaviour increases. Moreover, these results suggest that the thermal imbalances are sufficient to predominate on the anisotropy energy barrier for the nanomagnetic metal oxides, as a result, allows the magnetization to change the path in an instant [26,27]. As there can be no proof of additional phase or impurity in the prepared nanostructures in the present study and we thought that the oxygen vacancy should be the factor behind ferromagnetism in pure Fe_3O_4 and Nd-doped Fe_3O_4 nanoparticles. It can be clearly seen from the earlier discussion that the Nd dopant in Fe_3O_4 nanoparticles improves the ferromagnetic nature. An emitted free electron from the Nd (dopant), which can facilitate the oxygen vacancies formation. It may reduce the spin-spin inter-action between the Fe and Nd ions, which in turn reduces the formation of oxygen defect and could have reduced the saturation magnetization in the higher concentration of dopant. Pure Fe_3O_4 and Nd-doped Fe_3O_4 are dependent upon the porosity, domain size, the morphology of particle, crystalline anisotropy and grain size. This behaviour happens because of the interaction of the metals with oxygen within the sublattice for the spinel structure. The dislocations as well as defects in the crystal structure result in the decrease of coercivity values [28].

Catalytic activity studies: Selective oxidation of styrene to benzaldehyde is certainly a significant chemical reaction and synthesized aldehydes offer as a starting material for a range

TABLE-1
MAGNETIC PROPERTIES (MAGNETIZATION, REMANENCE AND COERCIVITY) OF PURE Fe_3O_4 AND Nd-DOPED Fe_3O_4

Samples	Hc (Oe)	Mr (emu/g)	Ms (emu/g)
Fe_3O_4	25.34	06.12	41.12
0.01% Nd-doped Fe_3O_4	29.44	06.34	48.32
0.02% Nd-doped Fe_3O_4	32.56	07.54	50.34
0.03% Nd-doped Fe_3O_4	43.12	10.78	54.45
0.04% Nd-doped Fe_3O_4	53.55	13.68	65.32
0.05% Nd-doped Fe_3O_4	50.90	12.12	51.67

TABLE-2
EFFECT OF THE OXIDANT AND CATALYST TOWARDS THE CATALYTIC OXIDATION OF STYRENE TO BENZYL ALDEHYDE

Entry	Catalyst	Oxidant	Yield (%)
1	Fe_3O_4	TBHP	21.31
2	0.01% Nd-doped Fe_3O_4	TBHP	24,32
3	0.02% Nd-doped Fe_3O_4	TBHP	27.53
4	0.03% Nd-doped Fe_3O_4	TBHP	37.13
5	0.04% Nd-doped Fe_3O_4	TBHP	48,95
6	0.05% Nd-doped Fe_3O_4	TBHP	40.35
7	–	–	00.80
8	With catalyst	–	03.00
9	–	TBHP	04.50

of chemical products. So as to determine the ideal conditions of reaction, the oxidation of styrene had been used for example reaction. The reaction had been carried out in the absence of one of the components such as pure Fe_3O_4 or Nd-doped Fe_3O_4 catalyst, acetonitrile and hydrogen peroxide.

In the absence of the oxidant, pristine Fe_3O_4 and Nd-doped Fe_3O_4 showed only 3% yield of benzaldehyde and without the presence of the solvent showed 0.80% yield only. In the presence of H_2O_2 (oxidant) and without catalyst, benzaldehyde yield reaches up to 4.5% only. Therefore, it is proved that the oxidant and the catalyst are essential to produce more substantial yields of benzaldehyde. When the samples are prepared without plant extract, it showed a very low yield of benzaldehyde (Table-2). In present study, a maximum yield of 92.6% of benzaldehyde is obtained in the TBHP medium using pure Fe_3O_4 and Nd-doped Fe_3O_4 catalyst.

Reaction mechanism: A mechanism is recommended for the selective catalytic oxidation of styrene into benzaldehyde using single-crystalline Fe_3O_4 and Nd-doped Fe_3O_4 and illustrated in **Scheme-I**. The styrene and TBHP effectively dissolved in acetonitrile, because acetonitrile having a high dielectric constant and dipole moment. The acetonitrile as a solvent can initialize the TBHP (oxidant) by the formation of an anion (TBHP) in which nucleophilically attacks the nitrile to produce an intermediate (peroxycarboximidic acid), that can be become an effective agent for oxygen transfer. Simultaneously the TBHP (oxidant) along with the styrene (organic substrate) dissolves in an acetonitrile medium and formation of a homogeneous solution. The development of oxygen to the reaction system utilizing the oxidant kinds -Fe-Nd-OOH• types. These findings show that the phenyl ring and also the TBHP come in contact with the Nd and Fe atoms in Nd-doped Fe_3O_4 and also the internal active sites continue to be intact. The interaction of methylene group with the external metal ions of Nd-doped Fe_3O_4 can also be evidence in the adsorption of styrene on Nd-doped Fe_3O_4. However, the catalyst surface becomes regenerated by the action of the TBHP with the catalyst, that ends up with desorption of the benzaldehyde molecules, therefore preferring additional oxidation. Therefore, this method is of extreme attention in the selective oxidation of styrene to benzaldehyde. A green effective path had been therefore accomplished for the change of styrene to benzaldehyde utilizing a catalyst and also the selective formation of other aliphatic/aromatic aldehydes can also be anticipated [29-31].

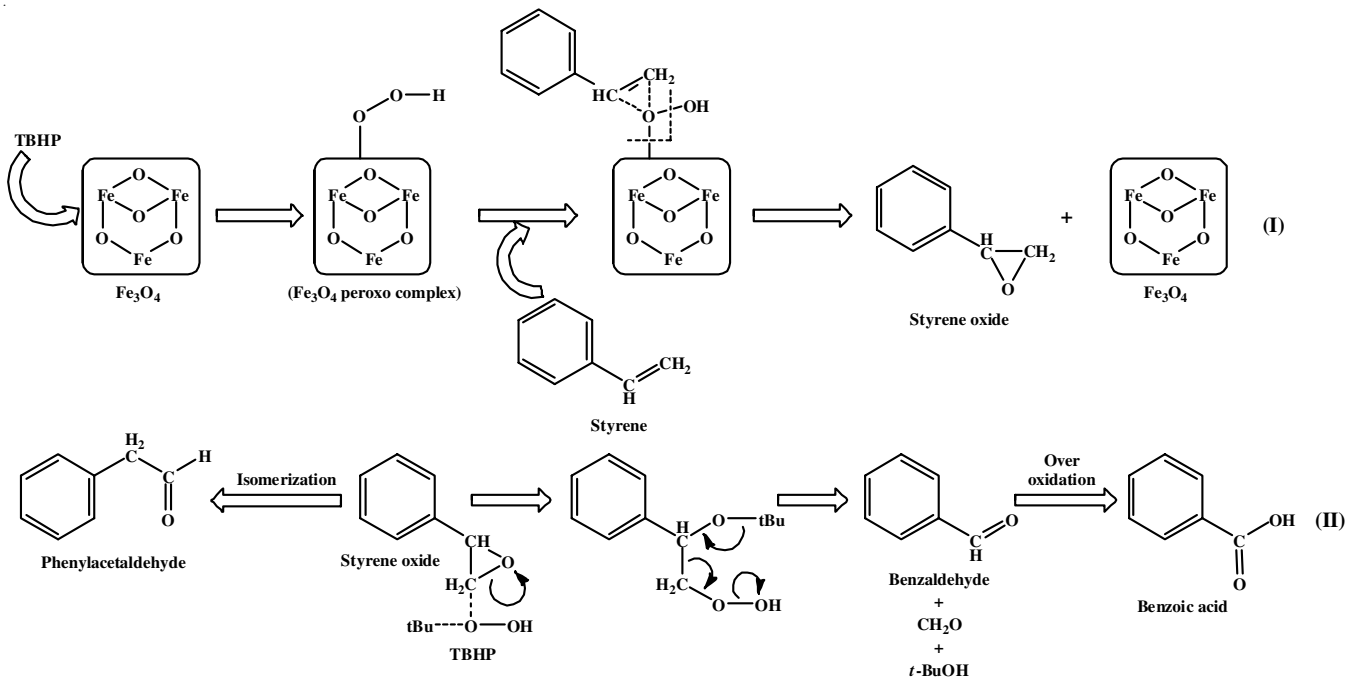

Scheme-I: Oxidation of benzyl alcohol using Nd doped Fe_3O_4 catalyst

Conclusion

This work clearly demonstrated that the nanoparticle size could be efficiently influenced by the doping of Nd on Fe_3O_4. Additionally, the impact of reaction time in the particle size and morphology of the samples had been examined. The particle dimensions are significant parameter, which extremely affects the properties of the catalysts. Its difference impacts the properties of samples directly, particularly while the particle size reduces to nanosize. Due to nanosized materials' unique properties were also compared to the bulk Fe_3O_4 materials. The influence of microwave technique in the magneto-optical morphological, structural, as well as catalytic performance in the selective oxidation of styrene into benzaldehyde were also examined. In summary, Nd-doped Fe_3O_4 nanoparticles with superior catalytic performance was attained by reduced crystal size and high surface area.

CONFLICT OF INTEREST

The authors declare that there is no conflict of interests regarding the publication of this article.

REFERENCES

1. C. Wang, H. Daimon and S. Sun, *Nano Lett.*, **9**, 1493 (2009); https://doi.org/10.1021/nl8034724
2. J. Guo, H. Gu, H. Wei, Q. Zhang, N. Haldolaarachchige, Y. Li, D.P. Young, S. Wei and Z. Guo, *J. Phys. Chem. C*, **117**, 10191 (2013); https://doi.org/10.1021/jp402236n
3. M. Bahiraei, M. Hangi and A. Rahbari, *Appl. Therm. Eng.*, **147**, 991 (2019); https://doi.org/10.1016/j.applthermaleng.2018.11.011
4. G.-X. Huang, C.-Y. Wang, C.-W. Yang, P.-C. Guo and H.-Q. Yu, *Environ. Sci. Technol.*, **51**, 12611 (2017); https://doi.org/10.1021/acs.est.7b03007
5. K.A. Stoerzinger, C.I. Pearce, T.C. Droubay, V. Shutthanandan, A. Shavorskiy, H. Bluhm and K.M. Rosso, *J. Phys. Chem. C*, **121**, 19288 (2017); https://doi.org/10.1021/acs.jpcc.7b06258
6. P. Yadoji, R. Peelamedu, D. Agrawal and R. Roy, *Mater. Sci. Eng. B*, **98**, 269 (2003); https://doi.org/10.1016/S0921-5107(03)00063-1
7. Y. Ma, H. Peng, J. Liu, Y. Wang, X. Hao, X. Feng, S.U. Khan, H. Tan and Y. Li, *Inorg. Chem.*, **57**, 4109 (2018); https://doi.org/10.1021/acs.inorgchem.8b00282
8. R. Hajian and A. Ehsanikhah, *Chem. Phys. Lett.*, **691**, 146 (2018); https://doi.org/10.1016/j.cplett.2017.11.009
9. F. Brühne and E. Wright, Benzaldehyde, in: Ullmann's Encyclopedia of Industrial Chemistry, edn 4, vol. 2, pp. 223-235 (2003).
10. C. Della Pina, E. Falletta and M. Rossi, *J. Catal.*, **260**, 384 (2008); https://doi.org/10.1016/j.jcat.2008.10.003
11. X. Wu, Z. Ding, N. Song, L. Li and W. Wang, *Ceram. Int.*, **42**, 4246 (2016); https://doi.org/10.1016/j.ceramint.2015.11.100
12. R.A. Reddy, K.R. Rao, B.R. Babu, G.K. Kumar, C. Rajesh, A. Chatterjee and N.K. Jyothi, *Rare Met.* (2019); https://doi.org/10.1007/s12598-019-01285-4
13. M.A. Almessiere, Y. Slimani, A.D. Korkmaz, S. Guner, M. Sertkol, S.E. Shirsath and A. Baykal, *Ultrason. Sonochem.*, **54**, 1 (2019); https://doi.org/10.1016/j.ultsonch.2019.02.022
14. M. Hashim, Alimuddin, S.E. Shirsath, S. Kumar, R. Kumar, A.S. Roy, J. Shah and R.K. Kotnala, *J. Alloys Compd.*, **549**, 348 (2013); https://doi.org/10.1016/j.jallcom.2012.08.039
15. N. Yasmin, I. Inam, I.A. Malik, M. Zahid, M.N. Ashiq, S. Abdulsatar, M. Safdar and M. Mirza, *Physica B*, **550**, 90 (2018); https://doi.org/10.1016/j.physb.2018.08.039
16. B. Choudhury and A. Choudhury, *Mater. Sci. Eng. B*, **178**, 794 (2013); https://doi.org/10.1016/j.mseb.2013.03.016
17. K. Mandal, S.P. Mandal, P. Agudo and M. Pal, *Appl. Surf. Sci.*, **182**, 386 (2001); https://doi.org/10.1016/S0169-4332(01)00455-X
18. C. Ragupathi, L.J. Kennedy and JJ. Vijaya, *Adv. Powder Technol.*, **25**, 267 (2014); https://doi.org/10.1016/j.apt.2013.04.013
19. Q. Zhang, M.F. Zhu, Q.H. Zhang, Y.G. Li and H.Z. Wang, *Compos. Sci. Technol.*, **69**, 633 (2009); https://doi.org/10.1016/j.compscitech.2008.12.011
20. A. Manikandan, J.J. Vijaya, L.J. Kennedy and M. Bououdina, *J. Mol. Struct.*, **1035**, 332 (2013); https://doi.org/10.1016/j.molstruc.2012.11.007
21. M.B. Sahana, C. Sudakar, G. Setzler, A. Dixit, J.S. Thakur, G. Lawes, R. Naik, V.M. Naik and P.P. Vaishnava, *Appl. Phys. Lett.*, **93**, 231909 (2008); https://doi.org/10.1063/1.3042163
22 A. Hajjaji, M. Gaidi, B. Bessais and M.A.E. Khakani, *Appl. Surf. Sci.*, **257**, 10351 (2011); https://doi.org/10.1016/j.apsusc.2011.06.072
23. M.M. Hassan, W. Khan, A. Azam and A.H. Naqvi, *J. Ind. Eng. Chem.*, **21**, 283 (2014); https://doi.org/10.1016/j.jiec.2014.01.047
24. R.K. Sendi and S. Mahmud, *Appl. Surf. Sci.*, **258**, 8026 (2012); https://doi.org/10.1016/j.apsusc.2012.04.163
25. Y. Shen, W. Li and T. Li, *Mater. Lett.*, **65**, 2956 (2011); https://doi.org/10.1016/j.matlet.2011.06.033
26. E. Rezlescu, N. Rezlescu, C. Pasnicu, M.L. Craus and P.D. Popa, *Cryst. Res. Technol.*, **31**, 343 (1996); https://doi.org/10.1002/crat.2170310313
27. S. Dietrich, S. Chandra, C. Georgi, S. Thomas, D. Makarov, S. Schulze, M. Hietschold, M. Albrecht, D. Bahadur and H. Lang, *Mater. Chem. Phys.*, **132**, 292 (2012); https://doi.org/10.1016/j.matchemphys.2011.11.015
28. Y. Köseoglu, A. Baykal, M.S. Toprak, F. Gözüak, A.C. Basaran and B. Aktas, *J. Alloys Compd.*, **462**, 209 (2008); https://doi.org/10.1016/j.jallcom.2007.07.121
29. C. Ragupathi, J.J. Vijaya and L.J. Kennedy, *Mater. Sci. Eng. B*, **184**, 18 (2014); https://doi.org/10.1016/j.mseb.2014.01.010
30. C. Ragupathi, J.J. Vijaya, L.J. Kennedy and M. Bououdina, *Mater. Sci. Semicond. Process.*, **24**, 146 (2014); https://doi.org/10.1016/j.mssp.2014.03.026
31. C. Ragupathi, J.J. Vijaya, S. Narayanan, S.K. Jesudoss and L.J. Kennedy, *Ceram. Int.*, **41**, 2069 (2015); https://doi.org/10.1016/j.ceramint.2014.10.002